Makara Journal of Technology

Volume 26 | Issue 1 Article 6

4-30-2022

Effects of Plasma Sintering on the Post TIG Weld Joint of Fe-15Cr-25Ni Austenitic Stainless Steel

Parikin Parikin
Research Center for Nuclear Reactor Technology, Nuclear Energy Research Organization, National Research and Innovation Agency, Puspiptek Area, Banten 15314, Indonesia, farihin@batan.go.id

Mohammad Dani
Research Center for Nuclear Reactor Technology, Nuclear Energy Research Organization, National Research and Innovation Agency, Puspiptek Area, Banten 15314, Indonesia

Arbi Dimyati
Research Center for Nuclear Reactor Technology, Nuclear Energy Research Organization, National Research and Innovation Agency, Puspiptek Area, Banten 15314, Indonesia

Andon Insani
Research Center for Radiation Detection Technology and Nuclear Analysis, Nuclear Energy Research Organization, National Research and Innovation Agency, Puspiptek Area, Banten 15314, Indonesia

Deswita Deswita
Research Center for Radiation Detection Technology and Nuclear Analysis, Nuclear Energy Research Organization, National Research and Innovation Agency, Puspiptek Area, Banten 15314, Indonesia

See next page for additional authors

Recommended Citation

Parikin, Parikin; Dani, Mohammad; Dimyati, Arbi; Insani, Andon; Deswita, Deswita; Aziz, Ferhat; Mardiyanto, Mardiyanto; Mustofa, Salim; Purwanto, Setyo; Adhika, Damar Rastri; Syahbuddin, Syahbuddin; and Huang, Ching An (2022) "Effects of Plasma Sintering on the Post TIG Weld Joint of Fe-15Cr-25Ni Austenitic Stainless Steel," *Makara Journal of Technology*: Vol. 26: Iss. 1, Article 6.
DOI: 10.7454/mst.v26i1.1577
Available at: https://scholarhub.ui.ac.id/mjt/vol26/iss1/6

Effects of Plasma Sintering on the Post TIG Weld Joint of Fe-15Cr-25Ni Austenitic Stainless Steel

Authors

Parikin Parikin, Mohammad Dani, Arbi Dimyati, Andon Insani, Deswita Deswita, Ferhat Aziz, Mardiyanto Mardiyanto, Salim Mustofa, Setyo Purwanto, Damar Rastri Adhika, Syahbuddin Syahbuddin, and Ching An Huang

Makara J. Technol. 26/1 (2022), 37−46
doi: 10.7454/mst.v26i1.1577

Effects of Plasma Sintering on the Post TIG Weld Joint of Fe-15Cr-25Ni Austenitic Stainless Steel

Parikin[1], Mohammad Dani[1], Arbi Dimyati[1], Andon Insani[2], Deswita[2], Ferhat Aziz[1], Mardiyanto[1], Salim Mustofa[3], Setyo Purwanto[4], Damar Rastri Adhika[5], Syahbuddin[6], and Ching An Huang[7]

1. Research Center for Nuclear Reactor Technology, Nuclear Energy Research Organization, National Research and Innovation Agency, Puspiptek Area, Banten 15314, Indonesia
2. Research Center for Radiation Detection Technology and Nuclear Analysis, Nuclear Energy Research Organization, National Research and Innovation Agency, Puspiptek Area, Banten 15314, Indonesia
3. Directorate of Research and Innovation Infrastructure Strengthening and Partnership, Deputy for Research and Innovation Infrastructure, National Research and Innovation Agency, Jakarta 10340, Indonesia
4. Research Center for Advanced Materials, Nanotechnology and Materials Research Organization, National Research and Innovation Agency, Puspiptek Area, Banten 15314, Indonesia
5. Research Center for Nanosciences and Nanotechnology, Institut Teknologi Bandung, Bandung 40132, Indonesia
6. Department of Mechanical Engineering, Faculty of Engineering, Universitas Pancasila, Srengseng Sawah, Jakarta 12640, Indonesia
7. Department of Mechanical Engineering, Chang Gung University, Taoyuan 33302, Taiwan

E-mail: ifyunasz@gmail.com

Abstract

Arc-plasma sintering (APS) for 5 s has been applied to the post tungsten inert gas (TIG) weld joint of Fe–15Cr–25Ni austenitic stainless steel (ASS). The treatment is intended to observe the effect of heat generated by plasma on micro-crystal structures around the fusion zone (FZ), especially internal stress relief in steel after being subjected to welding. The effect of stress relief in weld was measured using the neutron diffraction technique. ASS that is predominantly composed of Fe, Cr, and Ni elements, with contents of 57%, 15%, and 25%wt. respectively, was cut into two parts. Both parts were then welded with TIG without filler with a current and voltage of 60 A and 50 V, respectively. After APS for 5 s, the sample was characterized and analyzed using high-resolution powder neutron diffractometer at a high-temperature laboratory facility. The results show that the tensile residual stress decreased with the APS heat input. The residual stresses significantly decreased from 82.40 MPa to 1.21 MPa in the FZ and continued almost evenly from 65.92 MPa to 1.24 MPa in the heat-affected zone (HAZ). The residual stress is a tensile stress that can reduce the mechanical strength of materials. This condition is also applicable to applied loads. A microstructure gives a confirmation that the C element migrates from the FZ to HAZ. The content was very high in dark traces. The C element reacts to Cr and O to form chromium carbide ($Cr_{23}C_6$) and chromium carbonyl (CrC_6O_6), respectively. It rapidly migrates among its grain boundaries. It may also weaken materials and probably initiate intergranular cracks.

Abstrak

Pengaruh Sintering *Arc-Plasma* pada Sambungan Baja Tahan Karat Austenitik Fe–15Cr–25Ni Pasca Las TIG. Sintering *arc-plasma* selama 5 detik telah diterapkan pada sambungan las tungsten inert gas (TIG) pada baja tahan karat austenitik Fe–15Cr–25Ni. Perlakuan ini dimaksudkan untuk mengamati pengaruh panas yang ditimbulkan oleh plasma pada struktur kristal mikro di sekitar zona fusi, terutama pelepasan tegangan internal pada baja setelah pengelasan TIG. Pengaruh pengurangan stres setelah perlakuan panas plasma pasca-sinter diukur dengan menggunakan teknik difraksi neutron. Baja tahan karat Austenitik yang didominasi unsur Fe, Cr dan Ni dengan kandungan 57%, 15% dan 25%wt. masing-masing dipotong menjadi dua. Kedua bagian tersebut kemudian dilas dengan TIG tanpa filler dengan arus 60 Ampere dan tegangan 50 volt. Setelah disinter dengan plasma arc selama 5 detik, sampel dikarakterisasi dan dianalisis menggunakan difraktometer neutron serbuk resolusi tinggi (HRPD), SEM dan TEM di fasilitas laboratorium suhu tinggi. Hasil percobaan menunjukkan bahwa tegangan sisa tarik menurun dengan masukan panas sintering plasma busur. Tegangan sisa menurun secara signifikan dari sekitar 82,40 MPa menjadi 1,21 MPa di zona fusi dan berlanjut hampir merata di zona yang terkena panas sekitar 65,92 MPa menjadi 1,24 MPa. Tegangan sisa merupakan tegangan tarik yang dapat menurunkan kekuatan mekanik material karena meningkatkan beban yang diterapkan. Mikrostruktur memberikan

konfirmasi pengamatan. Elemen C bermigrasi dari fusi ke zona yang terpengaruh panas dan sangat tinggi di jalur gelap. Elemen C bereaksi dengan Cr dan O membentuk kromium karbida; Cr23C6 dan kromium karbonil; CrC6O6 masing-masing. Senyawa ini dapat dengan cepat bermigrasi di antara batas butir, sehingga dapat melemahkan bahan, bahkan boleh jadi memicu retakan intergranular.

Keywords: EDX, Fe–15Cr–25Ni austenitic stainless steel, HRPD, rietveld refinements, residual stress, SEM, TEM

1. Introduction

Stainless steels are generally selected on the basis of their corrosion resistance and mechanical properties. However, as the temperature of operating environments increases, these properties have quickly turn out to be the primary concern. Alloying designers give attention and closely examine the elevated-temperature properties for construction materials. As new processes are commercialized and as production capacities in existing facilities are increased, the temperature often becomes an important consideration in material selection. Stainless steel families that can flexibly meet the requirements of high-temperature services are in great demand by engineers. Four design factors are considered by engineers when choosing materials for service at elevated temperatures. These design factors are service life, allowable deformation, environment, and cost [1]. The first three factors are influenced by residual stress behaviors. The presence of residual stresses can weaken mechanically and chemically materials due to the magnitude and direction of residual stresses. Residual stresses can indirectly represent the material resistance to the environment and the increase in temperature corrosions. Hence, the presence of residual stresses may provide a long or short service life of materials.

Can the presence of residual stresses in materials be beneficial or detrimental to the strength of a component? The answer depends on the sign, magnitude, and type of load experienced by the components [2]. The distribution of residual stresses that adds to the used stresses can be detrimental, and the stresses against the direction of the used stresses can be advantageous. For repetitive or cyclic loads, the residual tensile (positive) stress can at times be very dangerous because it triggers the initiation and crack growth when fatigue stress is given. Manufacturing processes (screening and rolling) can leave a residual pressure (negative) that can hinder crack growth. This residual pressure is very much needed for components that experience repeated load types. For example, to increase the fatigue life of a material, thick steel plates are usually mechanized by the screening and rolling processes to generate compressive residual stresses. The effect of residual stresses on the behavior of a component is very interesting to be investigated and discovered because it can have a large effect on the strength of the component material. If a metal has been previously "work-hardened" (sometimes known as "cold-working"), then in terms of thermal treatment [3], the effect will depend on (i) how high the temperature is relative to the melting point of the metal and (ii) length of exposure to that temperature. Thus," "recovery" may just take place where there is just sufficient thermal energy to allow dislocations to move and rearrange themselves into new configurations and hence reduce residual stresses. High temperatures (1/3 to 1/2 of the melting point in Kelvin) will enable new strain-free metal grains to nucleate ("recrystallization"), consuming the original (stressed) structure and then subsequently grow in size ("grain growth").

Moreover, the quality of metal joining in the construction has been a major concern to the design factors, i.e., the welding process that connects one to another metal. Welding is a process that uses high heat (≥1000°) [4] to melt the parts together and allow them to cool, causing fusion. The application of weld causes the weld metal to heat up and melt around the edge metal connection. One that cannot be ignored during the thermal cycle is the material in heat-affected zones (HAZs) can undergo multiple phase transformations. This condition leads to the diversification of the structure between the weld metal and HAZ. It may result in various strain and stress conditions in the HAZ and outside areas. Hence, tracing the changes in the temperature allows one to determine the phase transformation and stressful state. The knowledge on the distribution and the value of permanent deformation and internal stress after welding are required because of their superposition with strains and stresses generated during the welding process. Moreover, the knowledge on changes in the thermo-mechanical state in precipitated steel elements is the basis for the rational design of the welding process [5]. Three principal zones are formed when welding is applied to the metal joining i.e., weld metal (fusion zone, FZ), HAZ, and base metal (BM). Because of the manufacturing process, weld joints are the weakest areas between them [6].

The hardness in the heat-affected material is not constant along the path, and the hardness varies from the BM to the maximum hardness zone in the HAZ. This hardness may be then considered for the heat treatments using arc-plasma sintering (APS). APS is a sintering technique used to improve the mechanical

properties of metals. APS is generally utilized to synthesize powder into bulk material [7]. The APS process operates at a very short time and is expected to produce little distortions, inducing less residual compressive stresses on the surface. The plasma sintering technique uses high temperatures (~2000°). This temperature can melt the steel for a long-time use. Therefore, sintering is performed in a short time (5 s) so that the sample material does not destruct. The sintering process is intended to examine the effect of the temperature on the healing of residual stresses in the weld joint area. APS is the first facility developed at the Pusat Sains dan Teknologi Bahan Maju–Badan Tenaga Nuklir Nasional (PSTBM–BATAN) material synthesis laboratory. The technique has proven to be successful in reducing time and energy consumptions in the manufacturing process. In this research, APS was tested to eliminate residual stresses due to the TIG welding process applied to the Fe–15Cr–25Ni austenitic stainless steel (ASS).

The measurements of residual stresses on the ASS with the no filler TIG welding process were conducted [2]. The results show that the largest residual stress occurred in the FZ, amounting to 82.40 MPa with a lattice stretching of 0.18%. Conversely, the values decreased to 65.92 MPa and a stretch of 0.14% in the HAZ. This residual stress is a tensile stress that can reduce the mechanical strength of the material because it adds to the applied loads. In this study, the welded sample was retreated with APS from a sample used in the literature [2]. The experiment was conducted to investigate the effect of APS for 5 s on the stress–strain curve and the microstructure evolution around the FZ of the above welded formation.

2. Experimental Procedure

The Fe–15Cr–25Ni ASS was synthesized by mixing and melting the scrap of granular chrome steel, plain carbon steel, FeSi75, low-carbon FeCr65, pure nickel, FeMn, slag remover, and pure aluminum using an inductance furnace at Bandung Polytechnic for Manufacturing. Aluminum was used for degassing. All fabrication processes were performed in accordance to the standard procedure of industrial production. In this work, small amounts of plain FeCr and FeC were added into an inductance furnace under an argon atmosphere for protection from oxidation. The mixture was then heated using 180 kW of power for 1 h until all the samples melt. Some of the mixture was slowly added to the melt to obtain the final composition. Pure FeMn, Ni, $FeCr_{65}$, and $FeSi_{75}$ were then poured into the melt at 1480 °.

The melt composition was inspected routinely and controlled at 1520 °C. The finished steel product consisted of 25.01 %wt. Ni and 15.42 %wt. Cr, giving this alloy high strength and high corrosion resistance. This steel also contained a small amount of 0.32 % wt. Mn, 0.005 %wt. Nb, and 0.02 %wt. Ti. All constituents of the ASS were measured through optical emission spectrometry. The chemical compositions of the ASS as-cast are listed in Table 1. All elements in the Fe–15Cr–25Ni ASS in this paper are stated in % by weight.

After hot rolling with a 70% reduction, steel plates with dimensions of 30 × 20 × 15 mm^3 were cut into two parts and then subjected to TIG welding with a current of 60 A and voltage of 50 V (heat input = 1500 J/mm), as described in a previous research [8]. The sample can be shown in Figure 1. Welding was performed by a welding engineer who fulfilled the requirements using special techniques based on the *Welding Procedure Specifications* made by professionals in BATAN.

Figure 2 shows the APS facility used in this study. The APS treatment is explained in detail and described by Dimyati *et al.* [9]. The TIG welded sample was located in a preheating chamber for plasma sintering. The temperature was set to a specific temperature (austenitic temperature: Tc ~1200°) [10] and remained constant for several seconds. The sample was then tempered to fix the microstructure for 5 s. To adjust the final hardness

Table 1. Chemical Composition of Austenitic Stainless Steel

Elemental Composition (%wt.)										
Fe	Cr	Ni	Si	C	Mn	Ti	S	P	Cu	Nb
57.74	15.43	25.10	0.96	0.34	0.32		less than 0.1			

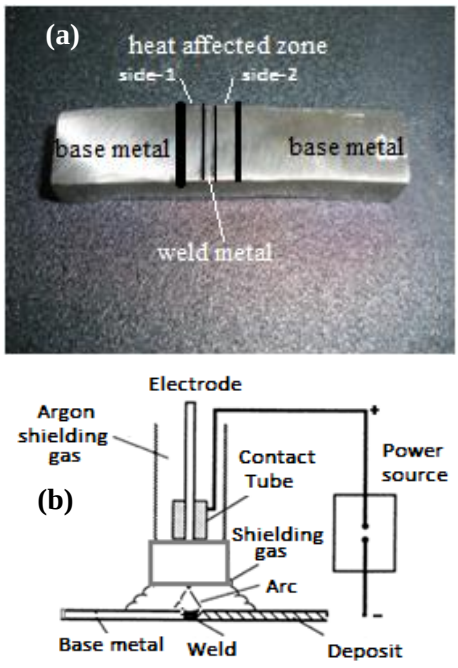

Figure 1. (a) TIG Welding Sample; (b) Plasma Spraying Schema [2]

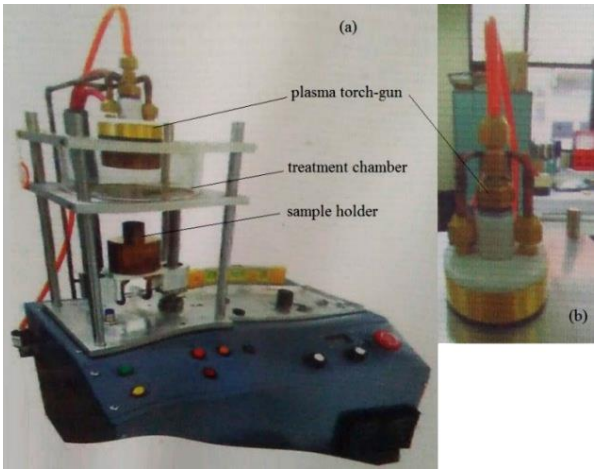

Figure 2. (a) Arc-plasma Sintering (APS) Facility in BATAN; (b) Plasma Torch Gun

of the sample, a temperature (below the melting point) stress-relieving treatment was performed in the chamber. Furthermore, the maximum hardness was located where the maximum deformation would occur under dynamic loads due to the high geometrical stress concentration. The aim of this heat treatment is not to recreate the real and complex thermal cycle induced by the welding process but to obtain specimens with mechanical properties close to those of an HAZ obtained by welding. A preliminary study was conducted to adjust the temperature (Tc) using an ampere regulator to obtain the correct austenite grain size in the material before the tempering. Hopefully, as the austenitic temperature rises, the hardness and grain size number must decrease. The HAZ microstructure and hardness were finally validated through a comparison with the HAZ obtained in the welded joint.

3. Results and Discussion

Neutron diffraction profiles. The high-resolution neutron powder diffractometer (HRPD) patterns of three measurable areas, i.e., the BM, HAZ, and FZ, shown in Figure 3, were run using a wavelength of approximately 1.82 Å. Five dominant diffraction peaks, typical for a face-centered cubic (*fcc*) crystal system, were entirely shown. Peaks appearing at successive diffractogram are correlated to the (111), (200), (220), (311), and (222) planes. These fields were numerically grouped according to odd or even numbers and diffracted at the consecutive 2θ angles, as listed in Table 2. Peak-to-background ratios can be clearly differentiated, which are the peak and background counts.

Rietveld refinements. Table 3 shows the specimen parameters and crystallographic data input in the calculation process. Data analysis was performed with Rietveld refinements and computed by the MAUD software [11]. The program can compute the powder diffraction data obtained using X-ray and neutron data. This program takes the initial crystallographic data to form the model pattern and scans neutron scattering chopped test specimens to form the standard pattern. In the calculation of the MAUD program, in the 2θ range, angles of 2.50°–162.50° were taken into consideration to obtain an optimal reference number value of goodness of fit (R_{wp}). Five iterations were carried out by the program in each MAUD calculations. Accordingly, goodness of fit of approximately 12% was obtained. Figure 3 displays the pattern for a Rietveld refinement of the FZ, HAZ, and BM, after the process of contaminant plastic tapes were excluded from the data. In the picture, there is one sign of line broadening, i.e., a line under standard patterns and models. This line indicates the position of the austenite phase (gamma-Fe) in the steel specimens of the Fe–15Cr–25Ni ASS.

The full pattern of standard profiles and smoothing are successively displayed in Figure 3. The refinements clearly show the structure of an *fcc* crystal system, from

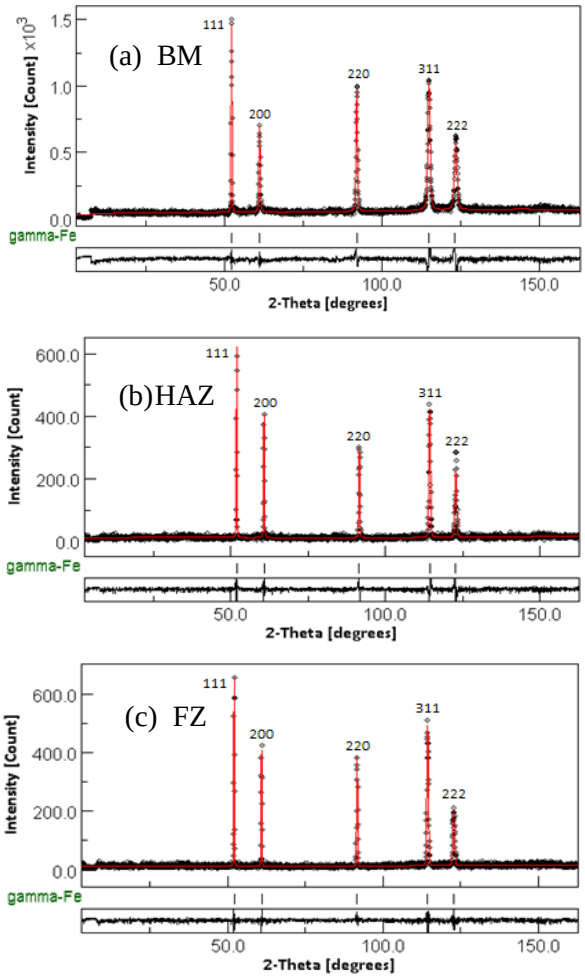

Figure 3. Neutron Diffraction Patterns and Rietvield Refinements of the (a) BM, (b) HAZ, and (c) FZ of the ASS. HRPD = 1.82 Å at the GA. Siwabessy Reactor

the figures reflecting the (111), (200), (220), (311), and
the figures reflecting the (111), (200), (220), (311), and (222) planes, which are patterned as all even or all odd. There is no evidence of any other phase in all the diffraction patterns found in each zone. Specimens treated with the TIG welding without filler can be assumed for the entire zone as a measure of the total *fcc*. The refinement was performed using single-phase models, i.e., the austenite phase (gamma-Fe) with the space group Fm3 m (I-225). The predicted initial lattice parameters for the austenite structure of the carbon content (C) in the steel specimens were conducted using the relation a (Å) = 3.555 + 0.106 x, with x as the weight percent of carbon [2]. The lattice parameter for the Fe–15Cr–25Ni steel with a carbon element content of 0.34 %wt. was 3.591 Å, used as an initial input into the Rietveld refinement calculation process by the MAUD program.

The refinement phase models shown in Table 3 are very much satisfactory with R_{wp} varying between 11.91% and 12.40%. The smoothing lattice parameter and peak positions for the austenite phase slightly shifted and gradually broadened from the zone to the measurement zones (FZ, HAZ, and BM) indicated from the full width half maximum (FWHM). Referring to the BM, the lattice strain ε can be obtained through the formulation of $\Delta a/a$ or $\Delta\theta = -2\,\varepsilon \tan\theta$ [12]. The parameters are listed in Table 4. The illustrations all of shifted and broadened peaks are representatively given by the (111) plane in Figure 4. Moving in the same direction, the (111) diffraction peaks shifted in the negative position from the HAZ to FZ, i.e., moving to a lower 2θ angle or approaching to the vertical axis. This condition causes crystal lattices to stretch in a positive direction and produce tensile tensions. The stresses were calculated using the formula of the hydrostatic tension: $\sigma = \varepsilon_{av} E/(1-\nu)$ [2].

Residual stresses. Residual stresses are normally found in machine/structure components. The cause of the residual stresses is the intensive accumulation of dislocations in one region as compared to other regions of the components.

Table 2. Rietveld Refinement Results of the TIG Welded Fe–15Cr–25Ni ASS Samples after Plasma Sintering for 5 s

Measurement Zone	Reflection (*hkl)*	2θ(°)	*a* (Å)	Goodness of Fit; R_{wp} (%)
BM	111	52.087	3.590719	12.12
	200	60.926		
	220	91.618		
	311	114.455		
	222	122.861		
HAZ	111	51.934	3.600626	12.40
	200	60.741		
	220	91.294		
	311	113.966		
	222	122.284		
FZ	111	51.938	3.600344	11.91
	200	60.747		
	220	91.304		
	311	113.983		
	222	122.302		

Table 3. Initial MAUD Refinement Parameters

Specimen	Reduction (%)	Crystallography
A2		Table Index: *I-225*
Austenitic steel	70	Crystal Structure: *FCC*
15%Cr–25%Ni		Space Group: *Fm3 m*
(70A2-APS5secs)		Lattice Parameters:
v = 0.293		$a = b = c$ = 3,591 Å
E =187 GPa		$\alpha = \beta = \gamma = 90°$

Table 4. Calculation Results of the Average Lattice Stress–Strain

Measurement Zones	Lattice Parameters (Å)	$2\theta_{111}$ (°)	FWHM (°)	Shifting $2\theta_{x\text{-}y\text{-}z}$ (°)	Average Lattice Strains (%)	Average Lattice Stresses (MPa)
BM*	3.59072	52.09	0.3326	0	0	0
HAZ	3.60063	51.93	0.2758	-0.1534	0.275	1.2428
FZ	3.60034	51.94	0.2589	-0.1494	0.267	1.2076

*ref

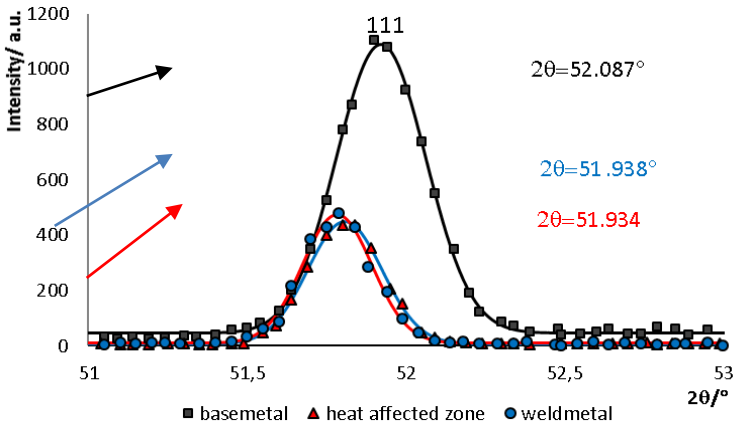

Figure 4. Shifting and Broadening (111) Plane of the Fe–15Cr–25Ni ASS around Post TIG Welding

In other words, the dislocation density can be higher in one region, i.e., surface crystalline, bulk crystalline, and around grain boundaries or second-phase particles, but not in other regions. Hence, to reduce the dislocation density, an appropriate heat treatment must be followed for a time period under a certain temperature. Knowing the chemical composition of a residual stressed component leads one to figure out the solution treatment of the component. Indeed, residual stresses can be harmful, especially when the dislocations emerge to the free surface, causing slip steps and then cracks in machine/structure components. Residual stresses will never be relieved completely, even by long heat treatments because removing all lattice defects is quite impossible. However, it is definitely possible to minimize first-order residual stresses into levels of less than 50 MPa in single-phase materials using a proper heat treatment [13]. The analytical results accurately tracked the experimental data for each of the heat treatments. The stabilization heat treatment significantly reduced residual stresses and subsequent machining distortions for fine grains, whereas coarse grains would require additional time or higher stabilization temperatures to attain the same degree of stress relief.

As reported before [2], the hydrostatic tension σ is directly proportional to the average strain in the formulation $\sigma = [E/(1-2\nu)]\ \varepsilon_{av}$, where E is the Young's modulus and the Poisson comparator ν is determined from the measurements of its own. The regression parameters for the sequential succession steel material are 187 GPa and 0.293, respectively. Figure 5a shows a graph of pre-APS 5 s residual stresses around the TIG weld with no filler, and Figure 5b shows a graph of post-APS 5 s residual stresses of the same sample. For the single-phase ASS (fcc), with integrated values of $\varepsilon_{av} = \varepsilon_a$, the tendency of the distribution of residual stresses from the structural material of austenitic results of rolling is the tensile stress. The rolling-up reduction of 70% generates a residual tensile stress of 9.7 MPa [2], whereas the

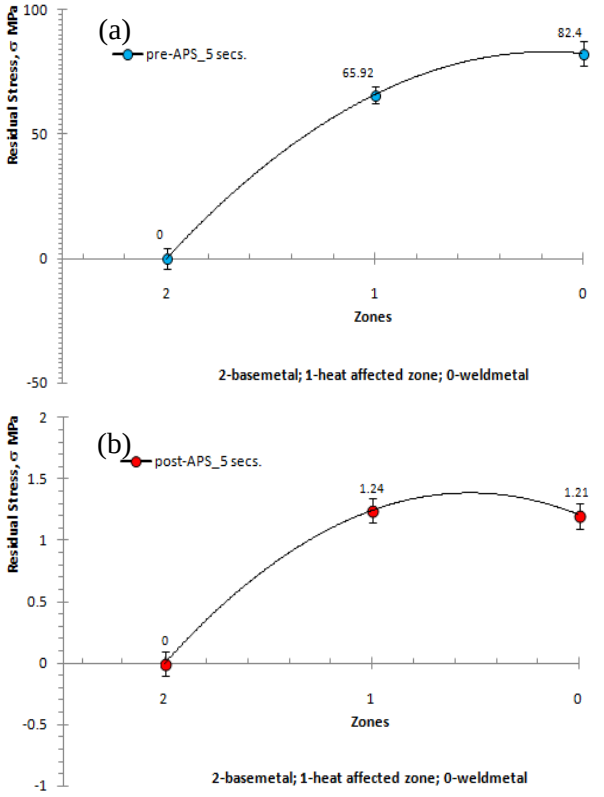

Figure 5. Residual Stresses around the TIG Welding of the Fe–15Cr–25Ni ASS: (a) Pre-APS 5 s and (b) Post-APS 5 s

residual stress due to welding heat added to the existing stress of 82.40 and 65.92 MPa in the weld metal and HAZ, respectively. The behavior of residual stresses of this material follows a strong dependency on the behavior of the crystal lattice strain (see Table 4) on average, as shown in Figure 5a–b. After 5 s of plasma sintering at the austenitic temperature, the number of residual stresses decreased by more than 98% in the two crucial regions, i.e., weld metal and HAZ.

Scanning electron microscopy–energy-dispersive X-ray analysis spectra. Referring to the BM in Figure 6a, the surface microstructure looks like a haystack in an elongated needle formation. The 70% reduction on cold–hot working (rolling) resulted in the formation of needles (elongated grains). The microstructure in the BM was composed of an evenly distributed austenitic phase, which was elongated along the rolling direction. The energy-dispersive X-ray (EDX) spectra shows that there is no carbon element emerging in the BM. Fe, Ni, and Cr elements were dominantly detected in the steel surface with compositions of 57.36, 25.69, and 16.08 %wt., respectively, and a small amount of Si element as a minor containment of 0.86 %wt. The BM was slightly finer than that of the FZ (weld metal).

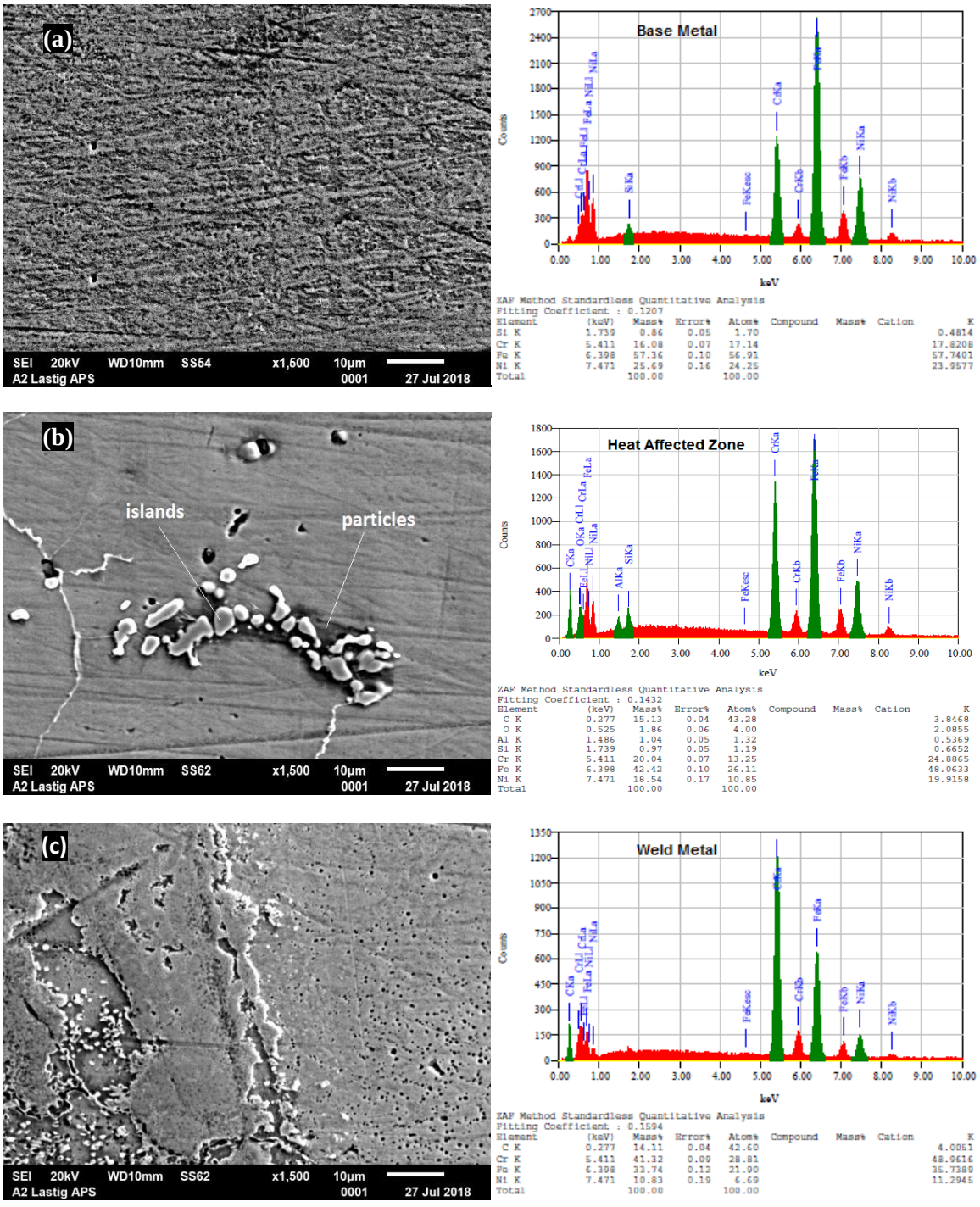

Figure 6. Microstructure and SEM–EDX Spectra in the (a) BM, (b) HAZ, and (c) FZ of the Fe–15Cr–25Ni ASS

As the peak temperature during welding in the HAZ ranged from just below the liquidus temperature to austenitization temperature, the transitions of the HAZ from the coarse-grain region to the fine-grain region and inter-critical region are described below. Furthermore, as shown in the HAZ and FZ spectra in Figure 6b–c, the surfaces are smooth enough. No elongated grain formations are shown. However, porosity is clearly displayed in the FZ surface. The EDX spectra show that the C elements emerge in the HAZ and FZ with the compositions of 15.13 and 14.11 %wt., respectively. The O element is contained in the HAZ of approximately 1.86 %wt. as black-spot particles. The oxidation process happens in this area, following island coagulations. Hence, the C elements may react with Cr or O elements to form the compound of $Cr_{23}C_6$ precipitates and CrC_6O_6 particles.

TEM observation. Figure 7 shows the TEM image at one of the fusion ends. The melt filler poured into the welding butt is clearly displayed. The melt filler is tilted sliding into the bottom of the "butt" valley, stretching from top to bottom. This is due to the fact that the lamellae preparation by the focused ion beam is sliced perpendicular to the welding direction.

With a magnification of 50 nm, three welding areas can be clearly distinguished: weld metal (FZ), HAZ, and BM. In the insert image, a magnification of 200 nm can show the microstructure between the FZ and HAZ. Tracing the results of the EDX mapping, the FZ and HAZ regions have chemical contents of Cr/C and Fe/Ni/Cr, respectively.

Figure 8(a) shows the TEM image of the FZ and HAZ in the ASS Fe–15Cr–25Ni welding joint. The melting direction of the filler material looks in the horizontal direction of the image. The TEM-EDX results in Figure 8(b) show the distribution of elements, indicating that the FZ is dominated by Cr and the HAZ consists of Fe, Cr, and Ni. High-C-concentration regions were identified inside the grains of the FZ and HAZ, such as on the area pointed by the yellow arrow in Figure 8(b). However, a high concentration of C was also found in the grain boundary area between the FZ and HAZ with the C concentration reaching 7.36% by weight, calculated from the gray spectrum in Figure 8(c). C concentrations are small in the FZ (4.02%) and HAZ (1.37%) calculated from the red and blue spectra in Figure 8(c), respectively. C is expected to form carbide compounds on grain boundaries and grain interior at the FZ and HAZ. In addition, the Cr concentration was very high at the FZ, reaching up to 75.42%, followed by 19.14% Fe and 1.42% Ni. In contrast to the FZ, the elements Fe, Cr, and Ni in the HAZ remained close to the element content in the Fe–15Cr–25Ni stainless steel, which are 60.14%, 14.91%, and 25.38%, respectively.

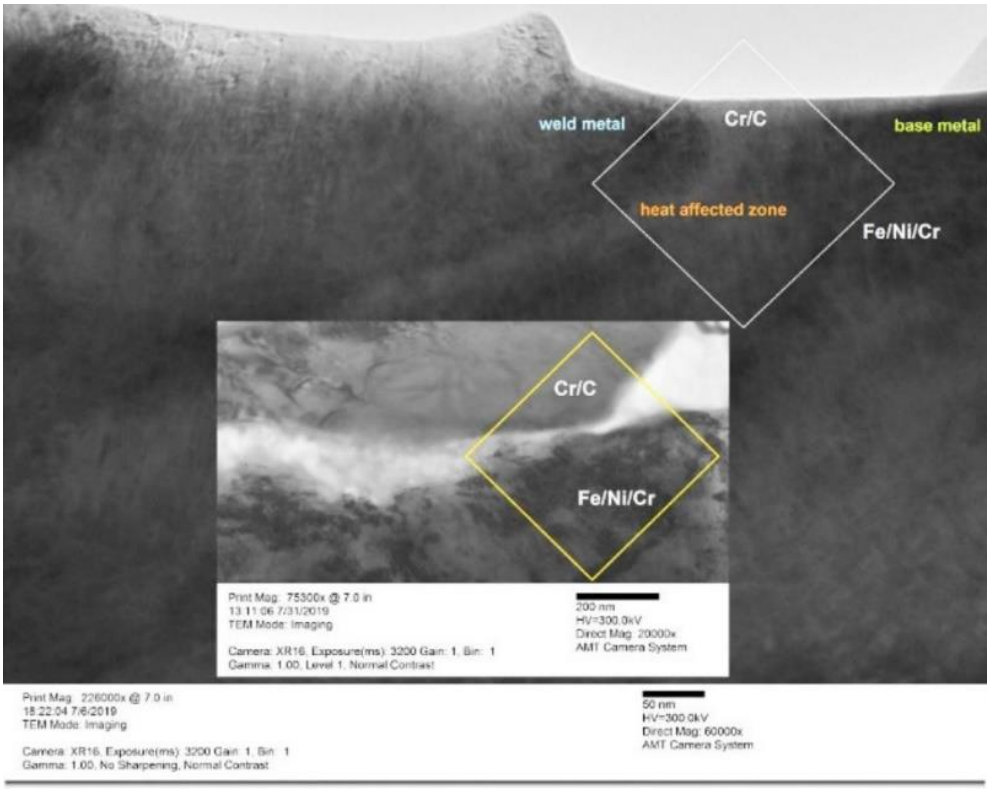

Figure 7. TEM Image of the Welding Zone, Showing the FZ, HAZ, and BM (50 nm). Insert Shows the Boundary between the FZ and HAZ (200 nm)

Referring to the Fe–Cr–Ni ternary-phase diagram [14], the phases that might be formed in the FZ and HAZ are α-Cr and γ-FeNi + α-Cr phases, respectively. In addition to these various phases, the carbide compounds formed in the grain interior and boundaries may cause the deformation of the surrounding area, forming residual stresses. After sintering, the number of dislocations in the FZ and HAZ is presumed to significantly decrease. Although carbide compounds were formed in the grains of the FZ and HAZ and also present in grain boundaries, their number was very small and spread in a very limited manner to certain areas. Thus, APS sintering for 5 min for the ASS Fe–15Cr–25Ni weld joint has a significant contribution to reducing the residual stress at the FZ and HAZ, as previously discussed.

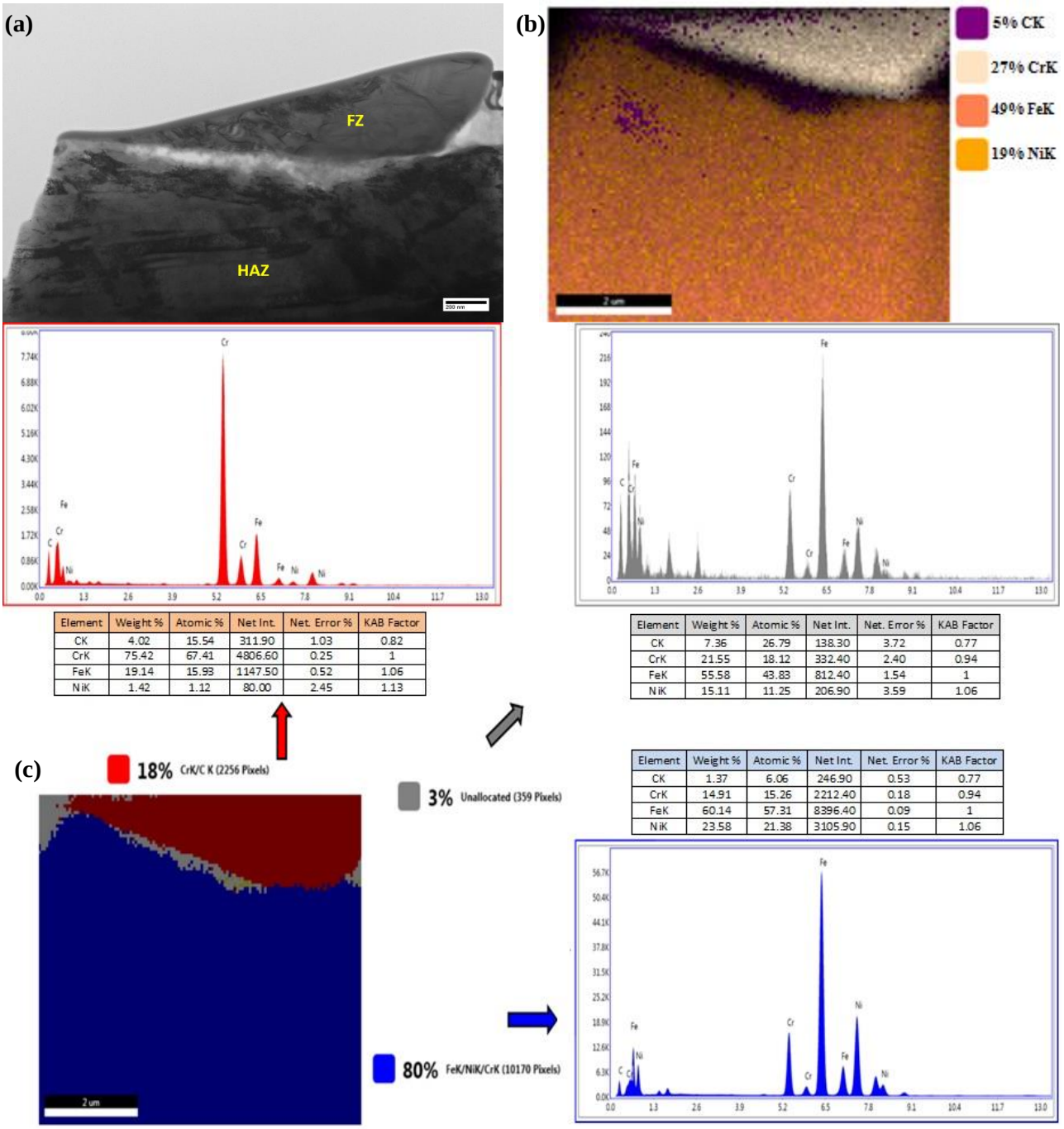

Figure 8. (a) TEM Image of the Welding Zone in the Fe–15Cr–25Ni ASS Sample after 5 s APS, (b) TEM-EDX Mapping Result Showing the Element Distribution on the area, and (c) TEM-EDX Mapping Result Showing the Classification of the area to be Three Regions with Different Element Distributions

4. Conclusions

As a summary, the heat treatments using the APS technique for 5 s can definitely refresh and heal the number of residual stresses in the post TIG welding of the Fe–15Cr–25Ni ASS. The residual stresses were reduced by almost 98% in the HAZ and FZ, i.e., from approximately 82.40 MPa to 1.21 MPa and from 65.92 MPa to 1.24 MPa, respectively. APS heat can minimize in part the accumulation of dislocations and defects in the weld joint grain boundaries of the Fe–15Cr–25Ni ASS to rearrange the atom structures in the crystals. This finding implies that weak materials may be cured from this side and the initiation of intergranular cracks, which rapidly migrate among its grain boundaries, can be eliminated.

5. Acknowledgment

The authors would like to express their gratitude to the heads and staffs of PSTBM and BSBM, Dr. Eng. Iwan Sumirat, Mr. Sumaryo, Mr. Rohmad Salam, and Mr. Agus Sujatno for their kindness and helps. The research was funded by the financial supports of DIPA 2018.

References

[1] E. Aniekan, O.E. Kelly, G. Abdulsamad. Int. J. Eng. Tech. 3/2 (2017) 50.
[2] Parikin, A.H. Ismoyo, R. Iskandar, A. Dimyati. Makara J. Technol. 21/2 (2017) 49.
[3] Y. Zhang, J. Li, C.B. Shi, Y.F. Qi, Q.T. Zhu. Met. 7/94 (2017) 16.
[4] Y.Y. Zhao, Y.S. Zhang, P.C. Wang. Mater. Sci. 96 (2017) 71.
[5] J. Winczek. Appl. Sci. 7/6 (2017) 19.
[6] J. Carrier, E. Markiewicz, G. Haugou, D. Lebaillif, N. Leconte, H. Naceur. Mech. Ind. 18/301 (2017) 9.
[7] H. Wahyudi, A. Dimyati, D. Sebayang. IOP Conf. Ser. Mater. Sci. Eng. 343 (2018) 6.
[8] Parikin, M. Dani, A.K. Rivai, A.H. Ismoyo, R. Iskandar, A. Dimyati. Makara J. Technol. 22/2 (2018) 66.
[9] A. Dimyati, N.R. Pratama, D.E. Jodi, B. Suharno. IOP Conf. Ser. Mater. Sci. Eng. 432 (2018) 7.
[10] P. Abbaszadeha, S. Kheirandisha, H. Saghafiana, M.H. Goodarzya. Mater. Res. 21/1 (2018) 8.
[11] L. Lutterotti. Dipartimento di Ingegneria dei Materiali, Universita di Trento 38050 Trento, Italy, 2006.
[12] Parikin, T.H. Priyanto, A.H. Ismoyo, M. Dani. Ind. J. Mater. Sci. 17/1 (2015) 22.
[13] L. Gurleyen, U. Ayata, B. Esteves, N. Cakicier. Maderas, Cienc. Tecnol. 19/2 (2017) 213.
[14] J. Wróbel, D.N. Manh, M.Y. Lavrentiev, M. Muzyk, S.L. Dudarev. Phys. Rev. B. 91/2 (2015) 31.